When do peripherally encoded memories generalize in visual working memory?

G. Kandemir & C.N.L. Olivers

Department of Experimental and Applied Psychology, Vrije Universiteit Amsterdam, The Netherlands

Running head: Foveal versus peripheral visual working memory

30/04/2024

Word count: 8068

Address correspondence to:

Güven Kandemir

Institute for Brain and Behaviour, Vrije Universiteit Amsterdam

Van der Boechorststraat 7, 1081 BT Amsterdam, The Netherlands

Email: g.kandemir@vu.nl

Telephone: +31 (0) 205981055

Abstract

Previous work has demonstrated that visual working memory of peripherally presented patterns transitions from location-specific to spatially generalized representations. It remains unclear what the temporal dynamics are of this generalization, and to which processing stages it is linked. Here we investigated the neural correlates of peripherally encoded memoranda before and after an item was selected for response, focusing on when the representation changes from a location-specific to a spatially generalized code. Thirty healthy participants memorized two orientations presented serially at 15 degrees eccentricity to the left and right of central fixation. One of the two items was subsequently cued, for which memory performance was then assessed. During the delays between each of these events, impulse signals were presented to trace memoranda in potentially activity-silent or activity-reduced states. Replicating prior findings, we observed that neural codes transitioned from dynamic, location-specific states to spatially and temporally generalized stable states post-encoding, here emerging from about 400 ms onwards. Importantly, this already occurred during maintenance, prior to selection of the response-relevant item. After the cue, first the location, and then the identity of the cued item emerged in the signal, suggesting that, despite the by then generalized code, location remained a useful basis for selection. The results suggest that spatial generalization is predominantly a maintenance-related rather than a selection-related process.

Key words: Visual working memory, peripheral vision, impulse perturbation, generalized representation, time course

Introduction

Visual working memory (VWM) enables us to maintain visual information in a directly accessible state, readily available to guide behavior (Cowan, 2001). The currently dominant theoretical view holds that VWM representations are closely tied to visual perception, such that memory storage corresponds to the sustained top-down recruitment of sensory representations in the absence of the original visual stimulation that activated those representations (e.g. Desimone & Duncan, 1995; D'Esposito, 2007; D'Esposito & Postle, 2015; Harrison & Tong, 2009; Olivers, 2008; Serences, 2016; Serences et al., 2009). At the same time, evidence indicates that feature representations held in VWM generalize beyond the neural populations activated by the percept itself, as functional imaging studies have revealed feature-sensitive pattern activity in areas other than the stimulated location (Ester et al., 2009; Jehee et al., 2011; Serences & Boynton, 2007). This generalization of feature-based activity in VWM beyond the stimulated location may reflect the recruitment of additional resources at the sensory level, the development of a common higher-order code, or both.

Relatively little is known about the time course of such VWM generalization. So far the bulk of studies used fMRI as the main technique, which is not optimal for exposing the dynamics of cognitive processes at a sub-second scale. In a recent study, we used EEG to compare VWM representations across the visual field (Kandemir & Olivers, 2024). On each trial, we asked participants to memorize the orientation of a single grating presented either at the fovea, or in the periphery at 15º eccentricity. After retaining this information for a couple of seconds, participants rotated a joystick to match a centrally presented probe grating with their memory. When we analysed the EEG using pattern classification techniques, we could distinguish three distinct phases. First, during the sensory encoding phase, the presented orientation could be decoded from central, but not from peripheral signals. Presumably the lack of a decodable signal for patterns this far into the periphery is caused by the folding of early

visual cortex into the calcarine fissure (Seki et al., 1996). This also meant there was no measurable generalization between the central and peripheral locations, nor between the peripheral locations themselves. During a second phase, after the stimulus had disappeared, a sustained maintenance-related voltage signal carried feature-specific information, for both foveally and peripherally presented patterns. While foveal and peripheral items were decodable at equal strength during this maintenance period, this pattern remained location-specific, as it failed to generalize across locations. Then, after approximately 600 ms, a third phase emerged during which the location-specific voltage-based pattern waned, and instead the memorized orientation became decodable from alpha-band oscillations. Moreover, this time the pattern generalized across central and peripheral locations. Given that alpha oscillations have been associated with selection processes involving spatial attention and response selection, we hypothesized that the common code may have reflected the creation of a more functional, output-ready representation that was abstracted from the initial sensory code, and that may either entail the attentional selection of a response-relevant aspect of the stimulus, or even the selection of the planned response itself (cf. Bae & Luck, 2018; Cochrane & Green, 2023; Duan & Curtis, 2024; Henderson et al., 2022; Kandemir et al., 2024a; Kwak & Curtis, 2022; Mostert et al., 2018; Myers, et al., 2017; Olivers & Roelfsema, 2020; Panichello & Buschman, 2021; van Ede & Nobre, 2023). Thus, by looking at the time course of different EEG signals, we could track the transition from separate input-related memory traces to a common output-related code.

While our previous study showed that the time course of generalization is informative, it leaves some questions unanswered. First, alpha suppression has been linked to both sensory and response selection mechanisms (de Vries et al., 2018; Günseli et al., 2019; Hanslmayr, 2011; Klimesch, 2012; Pavlov & Kotchoubey, 2020; van Ede et al., 2019), and it is unclear whether the generalization of signals we observed in the alpha band reflected a common code

at the sensory level or at the response level. For example, alpha modulations may have been related to either covert or overt spatial attention being directed towards the part of the edge of the grating patterns that is deemed most informative. Alternatively, alpha modulations may have been directly related to the direction in which observers planned to move the joystick. Given that there was a direct, one-to-one mapping between the orientation of the grating and the direction of the response, our analyses could not distinguish between these options. Second, the fact that we observed generalization for a late alpha signal, and not for the earlier, broadband voltage signal led us to propose that generalization is linked to an output-related representation (whether attention- or response-related), and probably not to a sensory representation. But this may have been calling the shots too early, as the task *allowed* for such output-related representations to be created in principle straightaway after encoding. On each trial, there was only a single grating to be encoded, and the stimulus itself already dictated what response had to be prepared. Thus the task potentially obscured, or even obviated the need for, a generalized code at the sensory level.

To investigate if generalization can occur in other stages than response preparation, and thus in other signals than (presumably) output-related alpha, we employed a retro-cue paradigm that allowed us to remove response-related confounds. Figure 1 illustrates a trial. Participants memorized two serially presented orientations, each presented at 15º eccentricity on opposite sides, and which were thus clearly spatially separated. Each of the patterns was followed by a substantial delay period, and only after the second delay, a cue indicated which of the two items was to be selected for report. The cue itself was a digit indicating the ordinal position of the relevant item, and thus did not carry any spatial information. Importantly, as before the cue it was not known which of the two patterns would become response-relevant, any generalization would thus be related to representations at pre-response levels of processing. The cue was followed by another delay, and the trial ended with a probe orientation. Here, participants

reported whether the probe was rotated clockwise or counterclockwise relative to the cued memorandum, and this direction was randomized. Thus, even after the cue, no concrete response could be prepared until the probe had appeared. If the generalization prior to response that we observed previously (Kandemir & Olivers, 2024) was indeed response-related, we should now no longer observe it. Any remaining generalization would thus still be related to sensory representations. Given that activity patterns may subside during the delays, we also included three impulse stimuli – one for each delay period – in an attempt to enhance our ability to trace memories in potentially activity-silent states (Kandemir & Akyürek, 2023;Kandemir et al., 2024a; 2024b; Stokes, 2015; Wolff et al., 2017; 2020a; 2020b).

Figure 1

A single trial.

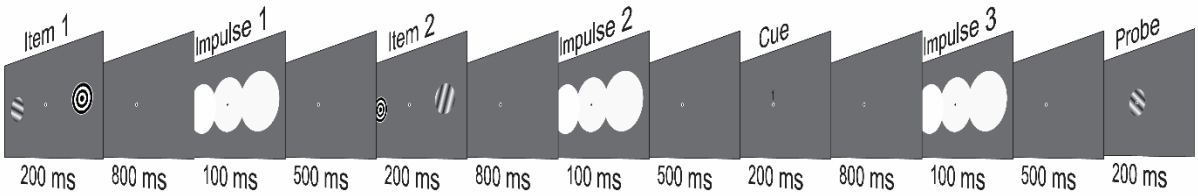

Note. Demonstration of a single trial where Item 1 is retrospectively cued, which would be part of a session during which Item 1 is always presented on the left and item 2 on the right and. Spatial position of items were switched between consecutive sessions and the order was balanced across participants. The task required participants to compare probe orientation relative to cued item and indicate relative direction.

Methods

Participants

The sample of participants consisted of thirty healthy young subjects (18 female, M_{Age} = 22.5, $s.d._{Age}$ = 4.75) who achieved at least 65% accuracy in a shorter prescreening version of the experiment (160 trials) conducted prior to the main experiment. Participants were paid 13 euros/hr. The sample size was the same as earlier studies to acquire enough power to

successfully discriminate orientations presented in the periphery (Kandemir & Olivers, 2024). Both prior to prescreening and the actual experiment participants were informed about the purpose and the design of the study as well as the data maintenance practices verbally and in writing. A written consent form was signed by participants to declare their compliance with participation and data storage practices. Procedures were approved by the Scientific and Ethics Review Board of the Faculty of Behavioral and Movement Sciences at VU University Amsterdam (protocol number VCWE-2021-173).

Stimuli and Apparatus

In each trial, two sinusoidal gratings were presented serially as memory items, each with a diameter of 5 degrees of visual angle (dva). The phase of the gratings varied randomly between 1 and 180 degrees for each trial, while the spatial frequency and contrast remained constant at 1. The orientations of the gratings were pseudo-randomly sampled from a set of eight discrete orientations, ranging from 11.25° to 168.75°, with an angular distance of 22.5° between them. The memory items were presented at an eccentricity of 15 dva to the left or right of the center of the screen (center-to-center distance). The location opposite the memory item was occupied by a bull's-eye symbol consisting of concentric black and white circles (5 dva in diameter), serving as a placeholder.

The cue was either the number 1 or 2, displayed in black 12-point Arial font, 0.25 dva above the fixation dot at the center, indicating the serial position of the cued memory item. The probe was a sinusoidal grating presented at the center of the screen with a random phase (1 to 180 degrees) and fixed contrast and spatial frequency (both set to 1). The diameter of the grating was 5 dva. The orientation of the probe always differed from the cued memory item in increments of +/- 6 °, 13 °, 21 °, 30 ° or 39 °.

Three impulse stimuli presented at different timepoints of the experiment were all identical and consisted of three overlapping white discs (RGB = 255, 255, 255). The discs had a diameter of 18.75 dva diameters and were centered at the origin, 10 dva left and right of the origin, respectively. As a result, the impulse stimuli covered spatial positions of both memory items as well as the region in between.

The feedback was a sad/happy smiley in light gray colour and had a diameter of 5 dva. The feedback was presented at the center of the screen briefly after a response. Throughout the experiment a gray background was maintained (RGB = 128, 128, 128;, 76.3 cd/m^2). A fixation dot formed by a black dot (0.3 dva diameter) surrounding a white circle (0.25 dva diameter), was always displayed at the center of the screen throughout a trial and participants were asked maintain their gaze fixated to this point at all times.

The experiment was programmed and run by Psychtoolbox extension for Matlab (Brainard, 1997; Kleiner et al., 2007). The stimuli were displayed on a 23.8 inch (60,452 cm on diagonal) ASUS ROG Strix XG248Q monitor with a resolution 1920 by 1080 pixels and a refresh rate of 240 Hz. The responses were collected by a regular keyboard where buttons ‘C’ and ‘M’ were pressed to indicate the direction of probe orientation. Eye position was monitored and recorded throughout a trial by a desktop-mounted Eyelink 1000 Plus at 1000 Hz sampling rate.

Procedure

The participants completed 1600 trials divided over 10 sessions, each lasting approximately 25 minutes and conducted consecutively on the same day. In each session, 160 trials were split into 10 blocks to minimize irritation of eyes from impulse stimuli. Participants self-initiated blocks but trials within block started automatically after each response. Participants could take breaks between blocks and sessions for self-determined durations to

combat fatigue. At the start of each session participants received instructions on blinking and gaze position as well as information about the spatial positions of Item 1 and Item 2, which were swapped in each session. The eye-tracker was re-calibrated using a 5-dot calibration method before the beginning of each session.

During the experiment, participants sat in a dimly lit room with their heads resting on a chinrest 60 cm away from the monitor. Figure 1 illustrates a trial. Each block began when the SPACE bar was pressed, followed by a 'Get Ready' message presented in 12-point black Arial font for 400 ms. Next, a blank screen was displayed for 600 ms. Afterwards, the fixation dot was presented until the end of trial. After 700 ms relative to the fixation dot onset, the first memory item and a placeholder at other location each 15 dva away from the center of the screen were presented for 200 ms. An 800 ms delay followed, after which Impulse 1 was presented for 100 ms. After another 500 ms delay, Item 2 was presented for 200 ms at the other location simultaneously with a placeholder at the position of previously presented Item 1. Another 800 ms delay ensued, followed by Impulse 2 for 100 ms duration, and then a 500 ms delay. Next, a number (1 or 2) was presented in black 12 point Arial font was displayed 0.25 dva above the fixation dot for 200 ms, cuing the serial position of the task-relevant item. After 800 ms delay, Impulse 3 was presented for 100 ms followed by a 500 ms delay. Finally, a probe consisting of a sinusoidal grating, was presented at the center of the screen for 200 ms. After the probe, a blank screen was presented until response. The probe was always different from the cued item. The task was to compare the orientation of the probe with the cued item. Participants responded by pressing 'C' or 'M' on the keyboard to indicate counter-clockwise and clockwise probe direction, respectively. Following their response, a smiley face (happy or sad) was displayed on the screen for 200 ms as feedback. The next trial began with the onset of the fixation cross after a random delay of 200 – 500 ms. Throughout the experiment simultaneous EEG data and eye position were monitored and recorded.

EEG Acquisition and Preprocessing

The 64 channel EEG was recorded at 1024 Hz via BioSemi Active 2 system. The electrodes were deployed according to international 10-20 system whereas four external electrodes were placed below and above the right eye (Vertical) and lateral to the external canthi (Horizontal) to record bipolar EOG. An additional pair external electrodes was placed on mastoids to serve as a reference after recording.

The preprocessing and visual checks of the EEG data were carried out using the freely available Matlab toolboxes, Fieldtrip (Oostenveld et al., 2011) and EEGLab (Delorme & Makeig, 2004). The data was first re-referenced to the average of mastoid electrodes and it was downsampled to 500 Hz. Next, a bandpass filter (0.1 Hz highpass – 40 Hz lowpass) was applied to the EEG. ICA was used to remove blink related components for each subject individually. Noisy channels were identified and replaced by spherical spline interpolation, with an average of 0.8 channels per subject. Next, data was epoched relative to stimuli onset times (-200– 1000 ms Item 1 and 2; -200 – 600 ms Impulses 1, 2 and 3; -200 – 1000 Cue). All epochs were visually inspected for eye and muscle artefacts, drifts and noise. Trials with artefacts were removed from analyses, leading to the exclusion of 8% of trials from each epoch for each participant.

Alpha power data was obtained by band-pass filtering (8 Hz highpass – 12 Hz lowpass) continuous, non-epoched data and applying Hilbert transformation. The absolute values were epoched using the same time windows as voltage data, and the same noisy electrodes and artefact containing trials were excluded from the analyses.

Behavioural Analyses

Behavioural analyses investigated performance in discriminating probe orientation relative to memory, using all trials. Response accuracy for all trials with the same probe deviation was averaged forming a probability distribution of correct response. Performance for

probe deviations in counter-clockwise direction was then multiplied by -1, so the entire distribution reflected the probability of reporting the probe as clockwise. These calculations were completed for the cued item to reveal overall performance, as well as separately for trials where item 1, item 2 or the Left and Right item was cued and compared to the probe.

A logistic distribution function was fitted to the observed probability of clockwise response for each subject when cued item was Item 1, 2, Item Left, or Item Right and slopes were estimated using the formula:

$$P_{clockwise} = \left(\frac{1}{1 + e^{-\beta(x-\theta)}}\right)$$

In the formula, x identifies probe deviation whereas the estimated θ is the threshold for clockwise-counterclockwise dichotomy and β is the slope. Estimated slopes were contrasted between conditions with pairwise t-test. The confidence interval for mean slope is calculated by bootstrapping (n_{perm} = 10 000).

Multivariate Analyses

Time-course analyses

The decoding procedure was adapted from earlier studies (Wolff et al., 2020a; 2020b)

Unless otherwise stated, all multivariate analyses were conducted using data from 19 posterior electrodes (PO7, PO3, POz, Pz, P1, P3, P5 ,P7 ,P9 ,Oz, P2, P4, P6, P8, O1, P10, PO8, PO4, O2), separately for each item location. For time-course analyses, the data was downsampled to 125 Hz to save computation time.

Next, the data was divided into eight folds with stratified sampling to ensure that the eight orientation conditions were equivalently represented in each fold. The training set consisted of data from seven folds, used to compute a covariance matrix with a shrinkage estimator (Ledoit & Wolf, 2004). Condition specific ERP was calculated for each channel as

patterns for orientation condition by averaging signal over training set trials. The number of trials in each condition was equalized by randomly sampling from the available trials to match the condition with the least trial count.

The difference between these patterns and each trial in test set (remaining fold) was calculated in Mahalanobis distance (De Maesschalck et al., 2000) with the logic that this value would be smallest if a trial belonged to one condition. The resultant distance measure were mean centered and their sign was reversed to associate higher values with higher similarity and these values are reported as similarity matrices.

To obtain a decoding accuracy value, trial specific distance measures were scaled by a cosine similarity function, convolving them with cosine function of orientations. The mean of this scaling operation yielded decoding accuracy at that time point in the trial. To mitigate variations in results due to trial selection, the entire decoding procedure was repeated 100 times, and the outputs were averaged for each participant across trials. The resulting output was smoothened using a Gaussian filter over the time dimension (kernel = 2 time points, 16 ms). Group data from all participants was then entered into statistical analyses.

For nominal conditions such as item location and cue type, the decoding procedure was identical except the final stage of scaling Mahalanobis distances. Instead of a cosine similarity, the decoding accuracy at a time point in a trial was calculated by taking the mean distance difference between conditions. The remainder of the analysis stayed the same.

When comparing representations across distinct memory items, epochs or conditions, training and test sets were formed from different conditions, unless the same conditions were tested in the same trials. In the latter case, the risk of confounding by autocorrelation would increase, due to which an eight-fold cross-validation procedure was used.

Dynamic changes in the neural code were investigated by training on the neural data at one time point and testing it on all other time points. For this, eight-fold cross-validated decoding procedure was applied. Temporal generalization analysis was repeated ten times to account for selection bias.

Critical time-window analyses

When more power was required to trace memory signals within a period of time, critical time-window analyses were conducted by combining data from all 19 electrodes and time points within the time window of interest into a single vector. Time of interest was determined as 100-400 ms window relative to item or impulse onset based on earlier practices. This method differs from time course decoding in how the data is prepared. First, instead of using a classical baseline, the mean activity on each electrode within the critical time-window was subtracted. Then, the data within this time window was downsampled to 100 Hz by creating 10 ms long snippets using a moving average. Next, the time and channel dimensions were concatenated, yielding a single spatio-temporal pattern with 570 features. This data was decoded using 8-fold cross-validation technique, with Mahalanobis distance as the measure of similarity, just as in time-course analyses.

Topography

The topographical distribution of the signal was inferred from electrode groups that could significantly be decoded for memory representations using a searchlight technique involving data from all 64 electrodes (van Ede et al, 2018). First, the mean activity within the time window of interest was subtracted. Next, the data was downsampled to 100 Hz by calculating the moving average over 10 ms windows. Before decoding, data from each electrode and two of its spatially closest neighbours were pooled over time to form spatio-temporal patterns for that specific region. The 8 fold cross-validated decoding was conducted

on this subset of electrodes, and the process was repeated until all electrodes were tested. This procedure was repeated 100 times to account for sampling bias. The output was then averaged over all trials and repetitions for each participant producing a single mean decoding value per electrode. Group level statistical analyses were conducted on this product.

Statistical analyses

The output of each decoding procedure was tested for statistical significance using non-parametric sign permutation tests. All reported tests were two-tailed unless specifically stated otherwise. For each analysis, a null distribution was generated using the group data, by randomly flipping the sign of the mean decoding accuracy for each participant 100 000 times with a probability of 0.5 and averaging the output. The group level data was compared to the null distribution and the proportion it corresponds to is taken as the respective *p* value. The cut-off for statistical significance was pre-determined at 0.05.

For searchlight decoding, the same procedure was applied at the channel level, returning *p* values for each channel across participants as channels with $p < 0.05$ were considered as electrodes significantly contributing to the memory classification. For the time-course data, null distributions were formed and contrasted at each time point and cluster correction with a cut-off of 0.05 was used to control for inflated chances of false positives.

Results

Behavioural Results

The overall mean response accuracy was 80.7% (sd = 6.14 %). Figure 2 shows the probabilities of reporting a clockwise deviation averaged across participants, as a function of the true deviation, serial position (Item 1, Item 2; Figure 2A) and location (Item Left, Item Right; Figure 2B), together with the best fitting psychometric function. Participants performed better when an item was shown second (Mean slope item 1: $\beta = 0.076$; item 2: $\beta = 0.099$, $p <$

0.001), which probably reflects a recency effect. There was no difference in performance for items presented on the left and right (Mean slope left: β = 0.88; right: β = 0.86, *p* = 0.26).

Figure 2

Average probability of responding "clockwise", split for item 1 and 2 (A), or split for left and right position (B), as a function of the true deviation of the probe from the target.

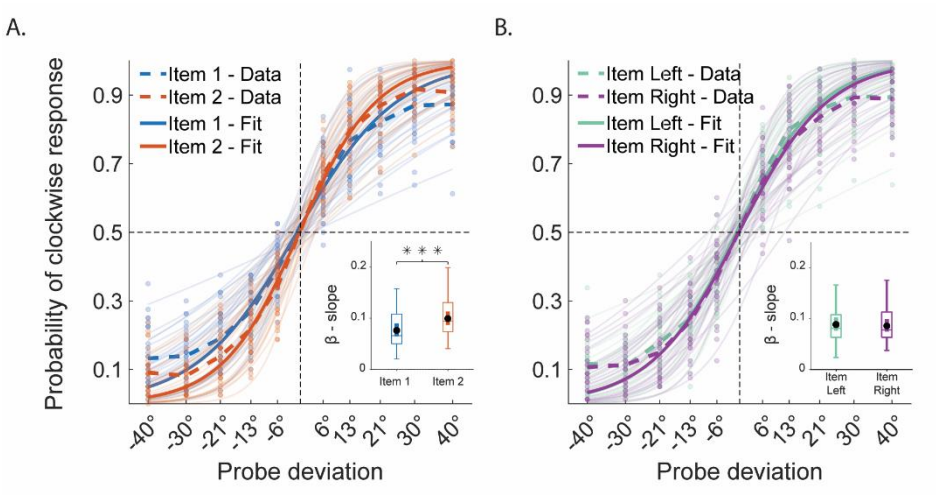

Note. A. The mean probability of responding clockwise to the probe, split up for Item 1 (blue) and Item 2 (orange). B. The same but split up for items on the left (green) versus right (purple) side of the display Solid lines show the overall logistic fit for Item Left (green-solid) and Item Right (purple-solid) estimated using the average of individual parameters. A-B. Dashed lines who the data, solid lines the logistic fit (the average of the individual parameters). Faded dots and lines reflect the individual data and logistic fits. Boxplots compare slopes (β) across conditions where black dots mark mean slope and asterisks indicate significant difference (*** = $p < 0.001$).

Decoding Results: Pre-cue phase

Initial encoding and maintenance. As Figure 3A shows, orientation could not be successfully decoded until about 140 ms from display onset, after which decoding strength waxed for about 500 ms and then slowly waned for another 500 ms (left panel of Figure 3A, Item 1, dark blue, 144 ms – 944 ms, $p < 0.001$; Item 2, orange, 136 ms – 992 ms, $p < 0.001$). Thus, as was the case for the peripheral stimuli in Kandemir and Olivers (2024), and in contrast to typical patterns for their more central stimuli, there was no strong stimulus-driven peak in decoding strength, but rather the signal developed in a more slowly and sustained fashion. Figure 3B shows the similarity matrices for Item 1 and 2, which reveal a parametric-looking

relationship between the neural signal and the angular differences, providing further evidence that it was an orientation-related signal that was being decoded.

A temporal generalization matrix averaged over memory items showed that while the initial approximate 400 ms period came with significant above-chance decoding at the diagonal (Figure 3C, where gray outlined regions indicate significant decoding above zero, $p < 0.05$), there was little in terms of off-diagonal signals, indicating that this early phase was characterized by a dynamic activation pattern. During this early phase, the topographical distribution of the decoded memory signal was strongly lateralized according to stimulus location, as was confirmed by searchlight analyses (Figure 3D, 100-400 ms window, all marked electrodes with decoding above zero, $p < 0.05$, one-tailed), consistent with a location-specific signal. In the later part of the epoch the signal became more stable, as it now generalized across time. During this phase, the topographical distribution was also more centralized on the posterior scalp (Figure 3D, 500-800 ms window, all marked electrodes with decoding above zero, $p < 0.05$, one-tailed), consistent with the possible emergence of a spatially generalized code – which we will address next.

Figure 3

Decoding of item 1 and 2 during and after stimulus encoding (A), representational similarity matrices (B), the temporal dynamics of memory representations over time (C), the topographical distribution of the memory signal during early 100-400 ms and 500-800 ms time-window (D) and generalization across locations (E) and serial positions (F) as a function of time.

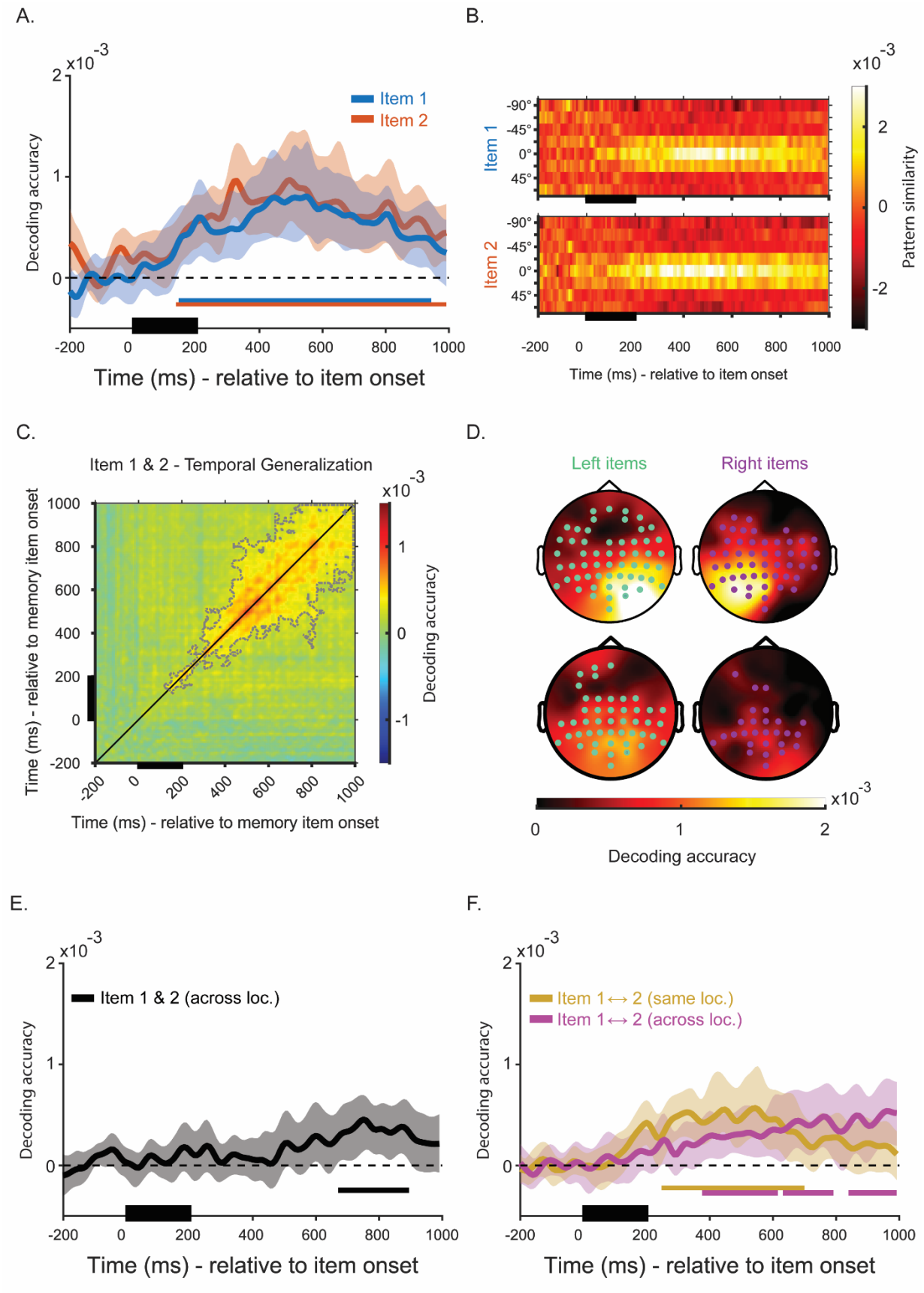
A.
x10^-3
Item 1
Item 2
Decoding accuracy
Time (ms) - relative to item onset
B.
x10^-3
Item 1
Item 2
-90°
-45°
0°
45°
Pattern similarity
Time (ms) - relative to item onset
C.
Item 1 & 2 - Temporal Generalization
x10^-3
Decoding accuracy
Time (ms) - relative to memory item onset
Time (ms) - relative to memory item onset
D.
Left items
Right items
x10^-3
Decoding accuracy
E.
x10^-3
Item 1 & 2 (across loc.)
Decoding accuracy
Time (ms) - relative to item onset
F.
x10^-3
Item 1↔2 (same loc.)
Item 1↔2 (across loc.)
Decoding accuracy
Time (ms) - relative to item onset

Note. Decoding of item 1 and 2 during encoding after Item 1 and 2 onset. **A.** Time-course decoding for Item 1 (dark blue), and 2 (orange). **B.** Representational similarity matrices for Item 1 and 2, reflecting parametric-looking relationship between orientations. **C.** Temporal generalization for memory items, averaged across serial positions. Initial period from 100 to 400 ms reveal a different temporal pattern in comparison to later period. Areas bordered by dotted lines show the time-zones with above zero decoding with statistical significance ($p < 0.05$). **D.** Topographic distribution of decoding, revealing electrode contributions for memory items on Left and Right during the initial 100-400 ms window as well as late 500-800 ms window, averaged across serial position, according to searchlight analysis. Brightness reflects the strength of decoding. Colored dots mark electrodes with above zero decoding accuracy with statistical significance ($p < 0.05$, one-tailed). **E.** The generalization of neural code for memory items across locations, when training on one spatial location (e.g. left) and testing on other (e.g. right, and vice versa) averaged over item 1 and 2. **F.** The generalization of neural code for memory items across serial positions, when training on Item 1 and testing on Item 2 (and vice versa) when these items were at the same location (mustard) and at opposite locations (pink). **A-F.** Solid lines reflect mean decoding accuracy as a function of time. Shades around solid lines mark 95 % C.I. Solid bars below baseline reflect the time-window with statistically significant decoding according to cluster-based permutation test ($p < 0.05$).

Spatial generalization. To assess whether decoding indeed generalized across spatial positions, we trained the classifier on data from one location and tested on data from the other (both ways, averaged for both items and both directions of decoding). This revealed that during the later part of the initial encoding and maintenance phase, the neural code indeed generalized across locations (Figure 3E, Item 1 & 2 cross-location, black, 672 – 896 ms relative to item onset, $p < 0.019$). When considering items individually, this generalization reached statistical significance for Item 1, whereas for Item 2 the same pattern was there but not significant (see Supplement, Figure S1A; Item 1, dark blue, 680 – 896 ms relative to item 1 onset, $p < 0.013$).

To assess whether spatial generalization also occurred between the two serial positions, we trained the classifier on Item 1 and tested on Item 2, and vice versa. This again revealed a transition from a relatively early phase of spatially specific patterns (Figure 3F, Item 1 ↔ 2 at same location, yellow, 248-704 ms relative to item onset, $p = 0.003$) to a later phase of spatially generalized patterns (Figure 4B, Item 1 ↔ 2 across location, pink, 368-608 ms, $p = 0.025$; 640-792 ms, $p = 0.030$; and 840-992 ms relative to item onset, $p = 0.028$). Collectively then, the results indicate a transformation from a temporally dynamic and spatially specific

representation into a temporally stable and spatially generalized representation, for both items. Importantly, this generalization occurs before the participant knows which item will become relevant for report.

Encoding and spatial generalization in alpha band. The presence of memory-related signals in the alpha band were investigated by decoding alpha power for Item 1 and 2. Indeed, decodable signals associated with memories emerged in the later periods of the epoch, approximately 500 ms after the onset of each item (left panel of Figure 4A, Item 1, dark blue, 576 ms – 976 ms relative to Item 1 onset, $p = 0.001$; Item 2, orange, 584 ms – 992 ms relative to Item 2 onset, $p = 0.002$). Importantly though, this signal was location-specific and did not generalize when we trained it on one location and tested on another (right panel of Figure 4B., Memory items, black, *ns*).

Figure 4

Decoding of item 1 and 2 from alpha power (A), and the assessment generalization of this neural code across locations during encoding as a function of time (B).

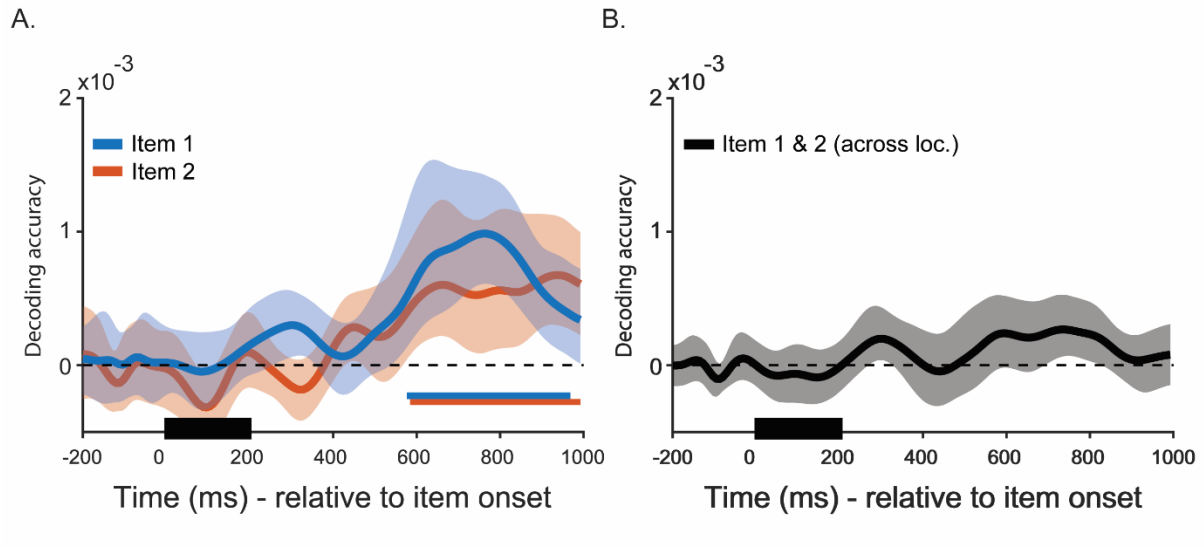

Note. The time course decoding of memory items from alpha power for item 1 and 2 (A), and the generalization of neural code across distinct spatial locations (B). **A.** Time-course decoding where the solid lines represent the mean decoding accuracy as a function of time when decoding is succeeded separately for each encoding location. Solid bars below baseline mark the time-window with statistically significant decoding according to cluster-based permutation test ($p < 0.05$). **B.** Time-course generalization where the solid line indicates the mean decoding

accuracy when training on one spatial location (e.g. left) and testing on other (e.g. right, and vice versa), averaged over item 1 and 2. The absence of a statistically significant period suggests that the alpha band activity correlating with memory features is specific to distinct encoding locations **A-B.** Shades around solid lines mark 95 % C.I.

Impulse-related signals. As activity tends to wane during VWM delay periods, we also included an impulse stimulus during the pre-selection delay, meant to revive any mnemonic patterns. Post impulse, we observed successful decoding of both memoranda (Figure 5A, Item 1, dark blue, 88 ms – 456 ms relative to Impulse 1 onset, $p = 0.004$; Item 2, orange, 104 ms – 592 ms relative to Item 2 onset, $p = 0.002$), with representational similarity matrices showing a parametric tuning of orientations (Figure 5B). At this post-impulse stage, the pattern was stable across time, as indicated by substantial temporal generalization (Figure 5C., gray dotted lines indicate decoding above zero, $p < 0.05$). Mostly central posterior electrodes contributed to item classification, regardless of the orientation stimulus having been presented on the left or right, which is again consistent with a spatially generalized code (Figure 5D., Left items, in green; Right items, in pink, $p < 0.05$, one-tailed). Cross-location decoding confirmed that activity patterns indeed generalized across space (Figure 5E., Item 1 & 2 (across loc.), black, 176 – 480 ms relative to Impulse 1&2 onset, $p = 0.008$). Figure S1B of the supplementary material shows the generalization for Item 1 and 2 individually at Impulse 1 and 2, respectively, while Figure S2 compares generalization between Item 1 and Item 2 at the same location and across locations.

Figure 5

Decoding of item 1 and 2 during maintenance after the presentation of impulse 1 and 2 (A), and their representational similarity matrices as a function of time (B), the temporal dynamics of memory representations over time (C), the topographical distribution of decoding within 100-400 ms time-window split over spatial positions (D) and the generalization of neural code across locations for Item 1 and 2 following the presentation of impulse 1 and 2 (E).

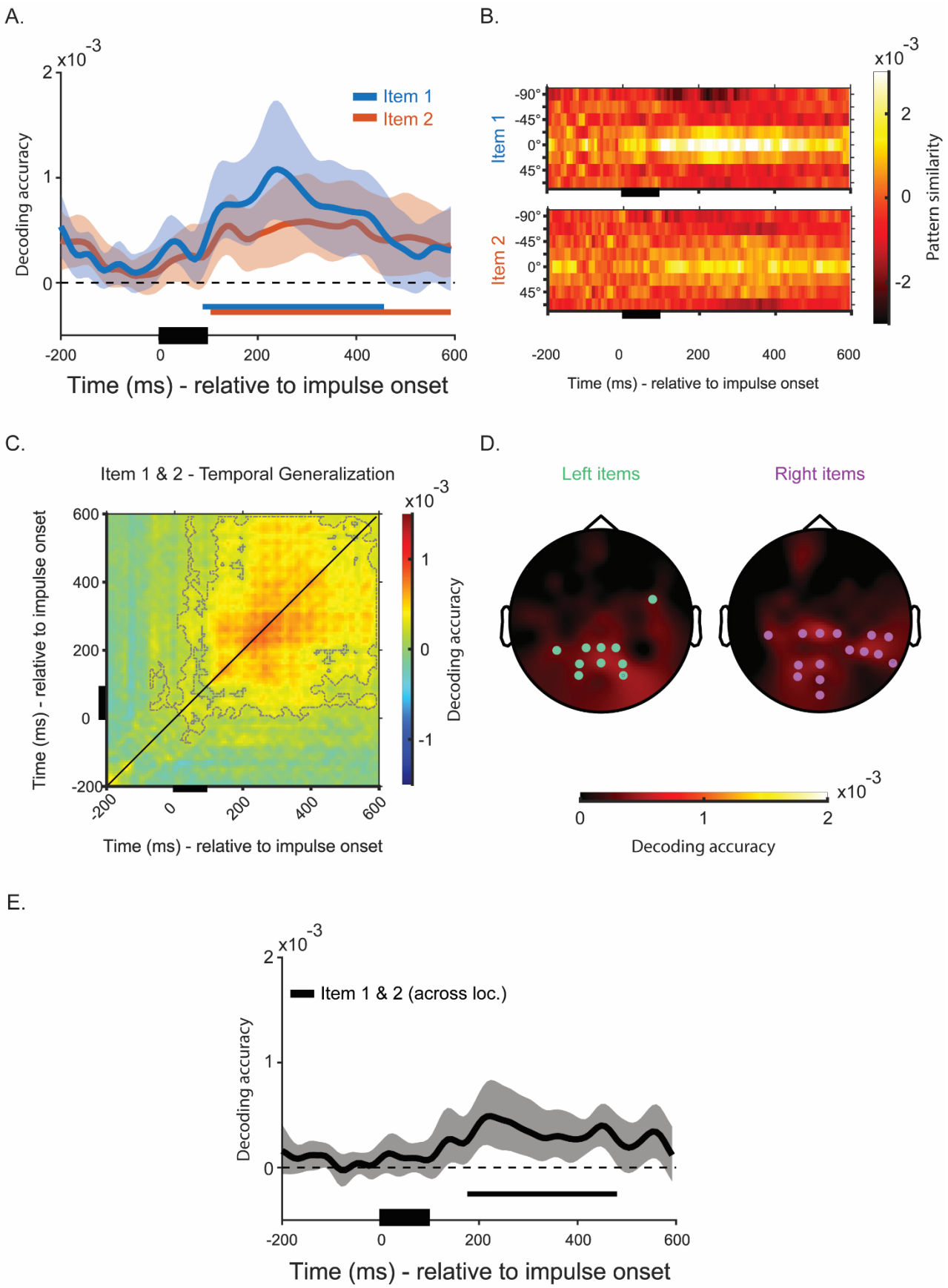
A.
x10^-3
Item 1
Item 2
Decoding accuracy
Time (ms) - relative to impulse onset
B.
x10^-3
Item 1
Item 2
-90°
-45°
0°
45°
Pattern similarity
Time (ms) - relative to impulse onset
C.
Item 1 & 2 - Temporal Generalization
x10^-3
Time (ms) - relative to impulse onset
Decoding accuracy
Time (ms) - relative to impulse onset
D.
Left items
Right items
x10^-3
Decoding accuracy
E.
x10^-3
Item 1 & 2 (across loc.)
Decoding accuracy
Time (ms) - relative to impulse onset

Note. Decoding of item 1 and 2 during maintenance, after impulse 1 and 2 presentation. **A.** Time-course decoding for Item 1 (dark blue), and 2 (orange). **B.** The similarity patterns for Item 1, and 2 as a function of time. Gradual change in distance measures as a function of angular distance reflects a parametric look-a-like relationship indicating orientation decoding for Item 1 and 2. **C.** Temporal generalization for memory items relative to impulse onset, averaged across serial position. Areas bordered by dotted lines show the time-zones with above zero decoding with statistical significance ($p < 0.05$). **D.** Topographic distribution of decoding accuracy revealing the contribution of electrodes for memory items on Left and Right according to searchlight analysis, averaged across serial position. Brightness reflects the strength of decoding. Colored dots mark electrodes with above zero decoding accuracy with statistical significance ($p < 0.05$). **E.** The timecourse of generalization of neural code for memory items across locations, when decoding by training on one spatial location (e.g. left) and testing on other (e.g. right) averaged over item 1 and 2 after impulse 1 and 2 presentation. **A-E**. The solid lines represent the mean decoding accuracy as a function of time whereas the shades surrounding them mark 95 % C.I. Solid bars below baseline reflect the time-window with statistically significant decoding according to cluster-based permutation test ($p < 0.05$).

We also assessed memory-related information in the post-impulse alpha-band signal, but none of the memory items were statistically traceable. Considering that both items were traceable prior to the impulse, we conclude that the impulse likely wiped out ongoing alpha band activity, consistent with what we observed in our previous study (Kandemir & Olivers, 2024).

Decoding results: Post-cue phase

Cue-related activity. In each trial, the serial position of one of the orientation memories was addressed by a retrospective cue. The type of cue (i.e. indicating Item 1 or Item 2) was traceable briefly after its onset (Figure 6A., Cue type, green, 88 – 992 ms relative to cue onset, $p < 0.001$). Moreover, the location of the cued item also became decodable (Figure 6A., Cued location, purple, 392 – 944 ms relative to cue onset, $p < 0.001$). We could not decode the orientation of the cued item from the subsequent voltage data. However, we could retrieve orientation information for the cued item at the end of the epoch, now from the alpha power data (Figure 6B, Cued item, red, 872 - 992 ms relative to cue onset, $p = 0.047$). No reliable spatial generalization was observed for this alpha signal though.

Figure 6

Decoding of cue type and cued location (A) and the cued as well as uncued item identity following the presentation of the cue as a function of time (B).

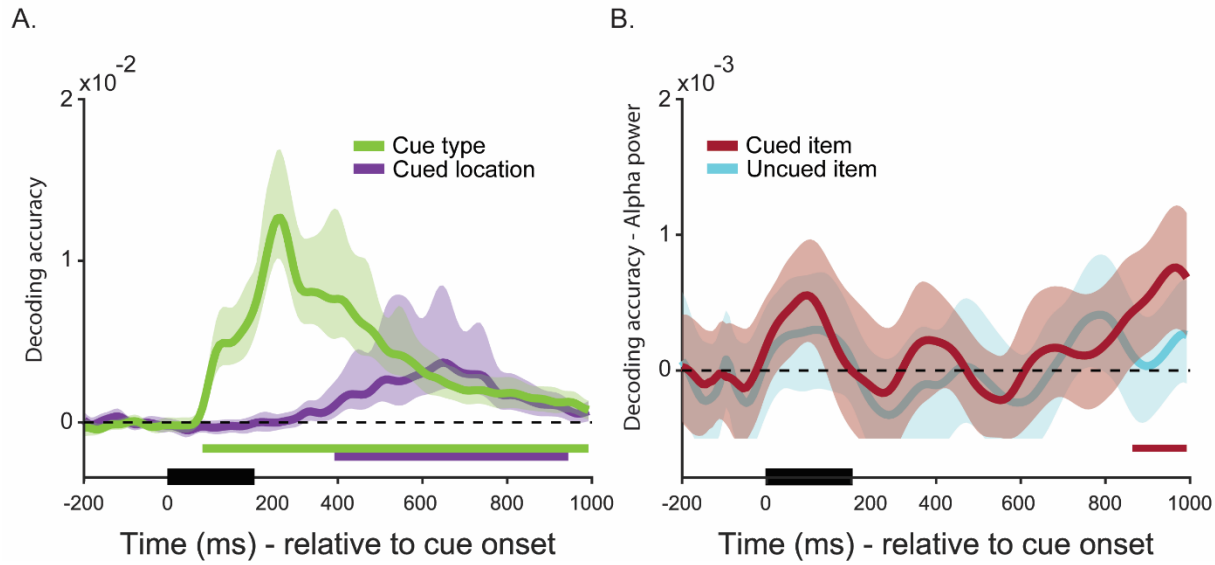

Note. Decoding at cue epoch. **A.** Time-course decoding of Cue type (green) indicating task relevant item order and Cued location (purple) corresponding to the spatial position of cued item at the periphery. **B.** Time-course decoding of alpha power data for cued (red) and uncued (cyan) item relative to cue onset. **A-B.** Solid lines represent the mean decoding accuracy whereas shadings mark 95 % C.I. Solid bars below baseline reflect the time-window with statistically significant decoding according to cluster-based permutation test ($p < 0.05$).

Figure 7

Decoding of cued and uncued item post-selection after the presentation of impulse 3 as a function of time (A), when data is combined over electrodes and time points within 100-400 ms time-window (B), generalization across locations when data was combined over time and electrode space (C), and the temporal dynamics of cued item over time (D).

A.

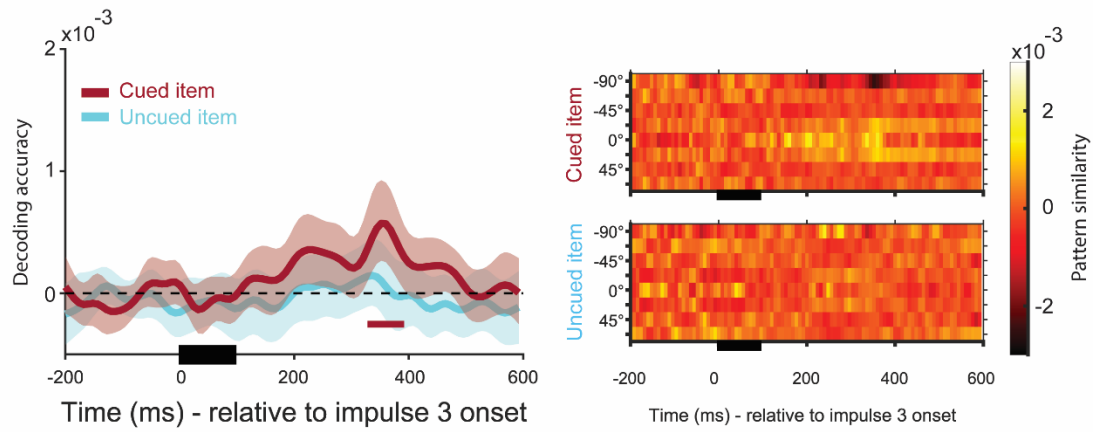
x10^-3
Cued item
Uncued item
Decoding accuracy
Time (ms) - relative to impulse 3 onset
Cued item
Uncued item
-90°
-45°
0°
45°
Pattern similarity
Time (ms) - relative to impulse 3 onset

B.

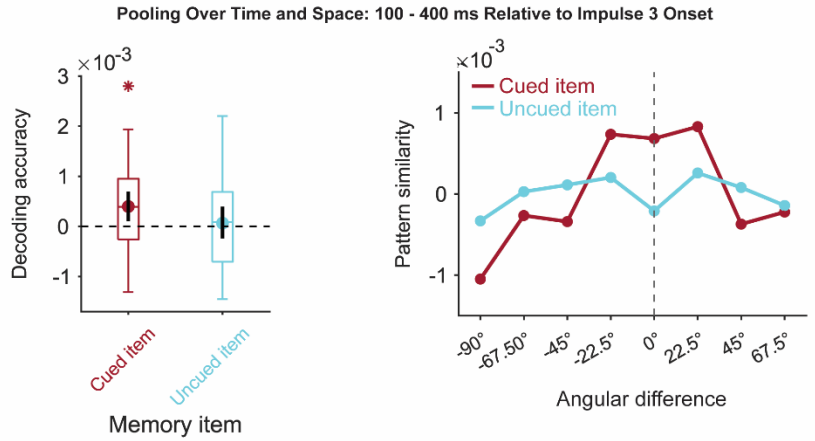
Pooling Over Time and Space: 100 - 400 ms Relative to Impulse 3 Onset
Decoding accuracy
Cued item
Uncued item
Memory item
Pattern similarity
Cued item
Uncued item
-90°
-67.50°
-45°
-22.5°
0°
22.5°
45°
67.5°
Angular difference

C.

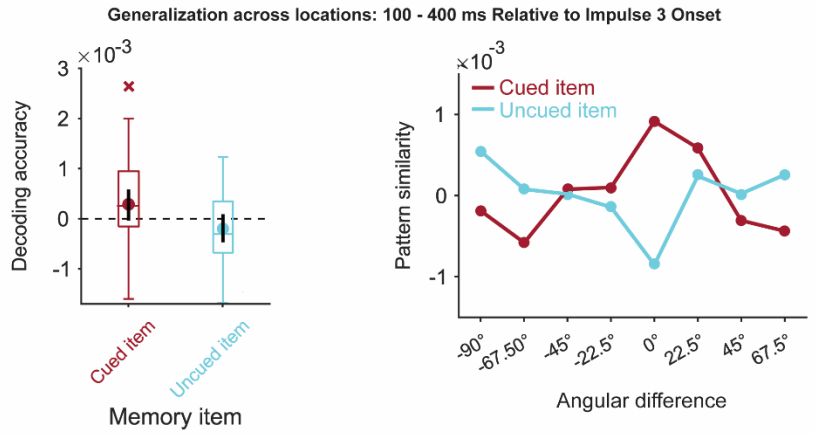
Generalization across locations: 100 - 400 ms Relative to Impulse 3 Onset
Decoding accuracy
Cued item
Uncued item
Memory item
Pattern similarity
Cued item
Uncued item
-90°
-67.50°
-45°
-22.5°
0°
22.5°
45°
67.5°
Angular difference

D.

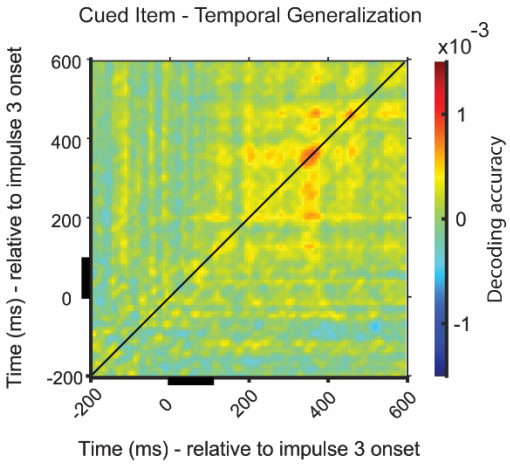
Cued Item - Temporal Generalization
Time (ms) - relative to impulse 3 onset
x10^-3
Decoding accuracy
Time (ms) - relative to impulse 3 onset

Note. Decoding of cued and uncued item post-selection after the presentation of Impulse 3. **A.** Time-course decoding where solid lines represent the mean decoding accuracy for cued (red) and uncued item (cyan). Shades around solid lines mark 95 % C.I. Solid bar below baseline reflects the time-window with statistically significant decoding according to cluster-based permutation test ($p < 0.05$). On the right, similarity patterns for cued and uncued items are presented. Gradual change in distance measures as a function of angular distance reflects a parametric look-a-like relationship indicating orientation decoding for the cued item, which is missing for uncued item **B.** Boxplots displaying decoding accuracy for the cued (red) and uncued item (cyan) with data combined over electrode space and across the time window of 100 – 400 ms relative to impulse 3. **C.** Boxplots displaying generalization across locations for the cued (red) and uncued item (cyan) with data pooled over electrodes and across the time window of 100 – 400 ms relative to impulse 3 when training on one location and testing on another. **B-C.** Large dots in in the middle of boxes mark mean values whereas black bars show 95 % C.I. The lower and upper borders of the boxes indicate 25th and 75th percentiles whereas whiskers mark +/- 1.5 IQR. Asterix indicate significant decoding (*** = $p < 0.001$; ** = $p < 0.01$; * = $p < 0.05$ with two-tailed test and, ^{x} = $p < 0.05$ with one-tailed test). On the right, similarity patterns reveal that when despite accurate decoding, discrimination of target from closest neighbours was not very successful for the cued item. **D.** Temporal dynamics of the cued item relative to impulse 3 onset. Although a generalized neural pattern is visible from yellow- reddish regions spreading across large time windows, no cluster was statistically significant.

Impulse-related signals. During the post-cue delay, another impulse signal was presented. Post impulse the orientation of the cued item identity could be successfully decoded from the voltage data (Figure 7A, Cued item, red, 328 - 392 ms relative to Impulse 3 onset, $p = 0.044$), while there was no reliable trace of the uncued item. To increase power we pooled over electrode space and time within a 100-400 ms time-window, by combining data from all 19 electrodes and time points into a single vector (Figure 7B, Cued item, red, 100 - 400 ms relative to Impulse 3 onset, $p = 0.013$; Uncued item, blue, ns). When we performed the same analysis but now decoding between locations rather than within, we found the same pattern, though not quite significant under a two-tailed test (Figure 7C, Cued item- across location generalization, 100-400 ms relative to Impulse 3, $p = 0.084$). When assessing generalization across time for the cued item, some visible off- diagonal regions appeared, though again too weak to yield any statistically significant clusters (Figure 7D). Overall then, we observed a relatively weak re-emergence of memorized information post impulse in the voltage signal, plus weak hints of generalization across space and time. Finally, we also decoded alpha power

for the cued and uncued items following Impulse 3. However, as for the preceding impulses, alpha power did not reflect orientation information for any of the items.

Discussion

Information in visual working memory spatially extends beyond the location of the encoded stimulus, suggesting a transition from that location-specific representations to a common code (Ester et al., 2009; Jehee et al., 2011; Kandemir & Olivers, 2024; Serences & Boynton, 2007). Here, using EEG, we further investigated the temporal dynamics of such transformation. In our previous study (Kandemir & Olivers, 2024), we observed such generalization to emerge from 800 ms after stimulus onset, and specifically within the alpha band signal. However, given the experimental procedure, this alpha-based generalization may have been driven by response preparation, as the response mapped one-to-one onto the stimulus. This may have obscured any generalization during stages prior to response selection. The current experiment required observers to remember two orientations, with one of them subsequently cued as relevant. Moreover, the eventual response mapping was independent of the stimulus. This way we clearly distinguished initial maintenance from selection for response. We replicated several findings of our earlier study (Kandemir & Olivers, 2024), yet also observed important differences. We outline the main observations here.

Behavioral performance was strong despite the peripheral location of the stimuli. Compared to typical VWM experiments, we presented the stimuli quite far out in terms of eccentricity (15º), to match with our previous study where we were primarily interested in the comparison between foveally and peripherally based memories (Kandemir & Olivers, 2024), and to ensure that the to-be-remembered patterns were initially far apart, thus facilitating the distinction between spatially specific and spatially generalized codes. Despite the eccentricity, behavioural performance was quite strong, suggesting that observers had relatively little

trouble perceiving and remembering the patterns. While performance did not differ for left and right, it was notably influenced by serial position, as on average performance was better for the second than for the first item. This difference may be attributed either to the second item interfering with the first, or the second item requiring a shorter maintenance period, and hence suffer less from decay or random noise. Both options would result in a recency effect (Broadbent & Broadbent, 1981; Schneegans & Bays, 2018; Wolff et al., 2020a).

The memoranda emerge only slowly in the EEG signal. The fact that our stimuli were presented at substantial eccentricity likely also caused a lack of clear decoding of stimulus-related sensory signals. The EEG did not reveal the early and typically strong onset-related transients in decoding that are observed for more centrally presented stimuli (e.g. King & Wyart, 2021; Myers et al., 2015; Wolff et al., 2017). This discrepancy is consistent with our earlier study where we observed that while foveally presented orientations became strongly and rapidly decodable from the EEG signal during the first 200 ms, peripherally presented orientations did not become traceable until later, through a slower and more sustained signal (Kandemir & Olivers, 2024). We hypothesize that the inability to decode the early sensory signals arises from the folding of primary visual cortex, with the periphery being represented inside the calcarine fissure (Seki et al., 1996), resulting in less detectable dipoles. The important implication is that the slower, sustained signal observed here must reflect a different signal than is initially triggered by the stimulus, and likely represents feedback activity higher up the visual hierarchy sustaining the actual memory. This is important to consider in the context of the sensory recruitment hypothesis, which, in its most extreme form, argues that visual working memory recruits the same representations as are used for the sensory experience. While our data do not reject the theory, they do indicate that EEG cannot be used to test its predictions where it concerns peripheral stimuli, as we show that their signals cannot be picked up from early visual areas (most notably V1).

It deserves mentioning that while in the current study the orientation information emerged quite slowly, it appeared to do so earlier than in our previous study (by 60 ms, taking the time point of statistical significance as a criterion, which is not without issues; Sassenhagen & Draschkow, 2019). Stimuli and eccentricity were identical in both studies. Moreover, compared to our previous study, the current study included fewer trials per condition, making an explanation in terms of statistical power less likely. Instead, the speeding may be due to differences in spatial attention to the periphery: In our earlier study, the presentation location varied randomly with equal probability between three locations (one central and two peripheral), whereas in our current study, the location of the peripheral item remained the same throughout a block. The predictability of the current stimulus location may well have sped up processing.

Orientation information transitions from temporally and spatially specific to temporally and spatially generalized patterns in voltage but not alpha-band signals. We found that activity patterns as extracted from the raw voltage signal gradually transitioned from being dynamic and location-specific to being temporally stable and spatially generalized, over the course of about one second. Also post impulse we observed the same generalized voltage signal. This shows that at least some of the orientation information of the memoranda generalized across space and time prior to the cue, and thus prior to any of the items being selected as response-relevant. Moreover, the temporal co-occurrence of the temporal and spatial generalization is striking. While the evidence is correlational, it raises the hypothesis that the generalized signal in both domains originates from the same stable representation.

Interestingly, the orientations could also be successfully decoded from power in the alpha-band, but this time the pattern did not generalize across space. Together, these findings provide a clear contrast with our previous results (Kandemir & Olivers, 2024), where we observed the opposite pattern: Generalization in alpha-band oscillations, but not in the voltage

signal. We believe that the crucial difference is that in our previous study there was only one stimulus to remember, and this stimulus also dictated the prospective response in a one-to-one fashion, as the memory test required observers to push a joystick in the direction of the orientation. Hence the memorandum could be in principle be recoded into a response-related signal straight after sensory encoding, which then emerged as a location-independent alpha signal. These signals may then have obscured or obfuscated the voltage-driven activity patterns that we observe here, when no response preparation was possible. This also means that these voltage-related patterns must represent pre-response processing levels, and we tentatively propose that they are thus more sensory-related, in line with the observed spread of orientation information in early visual cortex (Ester et al., 2009; Jehee et al., 2011; Kandemir & Olivers, 2024; Serences & Boynton, 2007). Our findings suggest that this generalization process starts to emerge about 400 ms post stimulus onset.

This leaves the question of what the location-specific alpha signal that we observed here then does reflect, if not response preparation. One possibility is that here it reflected attention being directed to relevant stimulus aspects, at the original stimulus location (cf. Bae & Luck, 2018; Fahrenfort et al., 2017). Interestingly, the location-specific alpha signal largely coincided in time with the emergence of the location-general voltage signal. This suggests the co-occurrence of two types information, one spatially specific and one spatially generalized. One hypothesis would be that one is causal to the other, as attending to the mental representation (as reflected in alpha) may lead to a generalized code (as reflected in voltage). But this is mere speculation at this stage and more research would be required.

Little generalization post selection. After the cue, orientation information again emerged within the alpha band, but we again found no evidence that this generalized across locations. On the contrary, it seems that the cue caused observers to mentally return to the original location, as was indicated by the strong post-cue location decoding. Note that the cue

itself only contained order information and no spatial information, and the original location was never relevant for the task. It thus seems that observers retained location information and may have used it as a retrieval cue, in line with other studies (de Vries & van Ede, 2025, van Ede et al., 2019). The decoded information in the alpha signal would then reflect mentally attending to the remembered orientation at its original location. Again, the fact that the alpha signal did not generalize here, but did in Kandemir and Olivers (2024) lends credence to the idea that in the latter study it reflected response selection processes (while here it reflects sensory selection).

Finally, after the cue we also observed significant decoding on the voltage-based signal, specifically post impulse. This may have reflected either a remnant of, or a restoration of, the pre-cue voltage signal that we observed. In line with this, this signal still showed signs of generalization, albeit statistically weaker than before the cue.

Conclusion. We conclude that task requirements play an important role in the generalization of memory representations – that is, which processing stage such generalization occurs, and in which signal this is then reflected. Overall, spatial generalization within VWM occurs quite rapidly, starting within about half a second, an can emerge from raw voltage (here) or alpha (Kandemir & Olivers, 2024), depending on the extent to which responses can be anticipated or not.

Data Availability

Processed and anonymized EEG and behavioural data reported in this manuscript, as well as MATLAB scripts and their output can be accessed via this link: (https://osf.io/jcg5k/?view_only=092daf47d6ea499785f08c1d382157af)

Acknowledgements

This project was funded by the Dutch Organization for Scientific Research (NWO; grant 453-16-002, to C.N.L.O.). We thank Ottavia Frangini for her help as a lab assistant during data collection and pre-processing.

References

Bae, G. Y., & Luck, S. J. (2018). Dissociable decoding of spatial attention and working memory from EEG oscillations and sustained potentials. *Journal of Neuroscience*, *38*(2):409-422. https://doi.org/10.1523/JNEUROSCI.2860-17.2017.

Brainard, D. H. (1997). The psychophysics toolbox. *Spatial Vision*, *10*(4), 433–436. https://doi.org/10.1163/156856897X00357.

Broadbent, D. E., & Broadbent, M. H. (1981). Recency effects in visual memory. *The Quarterly Journal of Experimental Psychology Section A*, *33*(1), 1-15. https://doi.org/10.1080/14640748108400762.

Cochrane, A., & Green, C. S. (2023). Working memory is supported by learning to represent items as actions. *Attention, Perception and Psychophysics*, *85*(5):1649-1660. https://doi.org/10.3758/s13414-023-02654-z

Cowan, N. (2001). The magical number 4 in short-term memory: A reconsideration of mental storage capacity. *Behavioral and Brain Sciences*, *24*(1), 87–185. https://doi.org/10.1017/S0140525X01003922

Delorme, A., & Makeig, S. (2004). EEGLAB: An open source toolbox for analysis of single-trial EEG dynamics including independent component analysis. *Journal of Neuroscience Methods*, *134*, 9–21. https://doi.org/10.1016/j.jneumeth.2003.10.009.

De Maesschalck, R., Jouan-Rimbaud, D., & Massart, D. L. (2000). The Mahalanobis distance. *Chemometrics and Intelligent Laboratory Systems*, *50*(1), 1–18. https://doi.org/10.1016/S0169-7439(99)00047-7

Desimone, R., & Duncan, J. (1995). Neural mechanisms of selective visual attention. *Annual Review of Neuroscience*, *18*(1), 193-222. https://doi.org/10.1146/annurev.ne.18.030195.001205

D'Esposito, M. (2007). From cognitive to neural models of working memory. *Philosophical transactions of the Royal Society of London, Biological Sciences*, *362*(1481), 761–772. https://doi.org/10.1098/rstb.2007.2086

D'Esposito, M., & Postle, B. R. (2015). The cognitive neuroscience of working memory. *Annual Review of Psychology*, *66*, 115–142. https://doi.org/10.1146/annurev-psych-010814-015031

de Vries, I. E. J., van Driel, J., Karacaoglu, M., & Olivers, C. N. L. (2018). Priority switches in visual working memory are supported by frontal delta and posterior alpha interactions. *Cerebral Cortex*, *28*(11), 4090–4104. https://doi.org/10.1016/j.cognition.2025.10611

de Vries, E., & van Ede, F. (2025). Microsaccades reveal preserved spatial organisation in visual working memory despite decay in location-based rehearsal. *Cognition*, *259*, 106111. https://doi.org/10.1523/ENEURO.0276-23.2023

Duan, Z., & Curtis, C. E. (2024). Visual working memories are abstractions of percepts. *eLife*, *13*, RP94191. https://doi.org/10.7554/eLife.94191.3

Ester, E. F., Serences, J. T., & Awh, E. (2009). Spatially global representations in human primary visual cortex during working memory maintenance. *Journal of Neuroscience*, *29*(48), 15258–15265. https://doi.org/10.1523/JNEUROSCI.4388-09.2009

Fahrenfort, J. J., Van Leeuwen, J., Foster, J. J., Awh, E., & Olivers, C. N. (2017). Working memory implements distinct maintenance mechanisms depending on task goals. *BioRxiv*, 162537. https://doi.org/10.1101/162537

Günseli, E., Fahrenfort, J. J., van Moorselaar, D., Daoultzis, K. C., Meeter M., & Olivers, C. N. L. (2019). EEG dynamics reveal a dissociation between storage and selective attention within working memory. *Scientific Reports*, *9*, 13499. https://doi.org/10.1038/s41598-019-49577-0

Hanslmayr, S. (2011). The role of alpha oscillations in temporal attention. *Brain Research Reviews*, *1*(2), 331–343. https://doi.org/10.1016/j.brainresrev.2011.04.002.

Harrison, S. A., & Tong, F. (2009). Decoding reveals the contents of visual working memory in early visual areas. *Nature*, *458*(7238), 632–635. https://doi.org/10.1038/nature07832

Henderson, M. M., Rademaker, R. L., & Serences, J. T. (2022). Flexible utilization of spatial- and motor-based codes for the storage of visuo-spatial information. *eLife*, *6*, e75688. https://doi.org/10.7554/eLife.75688

Jehee, J. F., Brady, D. K., & Tong, F. (2011). Attention improves encoding of task-relevant features in the human visual cortex. *Journal of Neuroscience*, *31*(22), 8210–8219. https://doi.org/10.1523/JNEUROSCI.6153-09.2011

Kandemir, G., & Akyürek, E. G. (2023). Impulse perturbation reveals cross-modal access to sensory working memory through learned associations. *NeuroImage*, *274*, 120156. https://doi.org/10.1016/j.neuroimage.2023.120156

Kandemir, G. & Olivers, C. (2024). Comparing neural correlates of memory encoding and maintenance for foveal and peripheral stimuli. *Journal of Cognitive Neuroscience*, *36*(9):1807-1826. https://doi.org/10.1162/jocn_a_02203

Kandemir, G., Wolff, M. J., Karabay, A., Stokes, M. G., Axmacher, N., & Akyürek, E. G. (2024a). Concurrent maintenance of both veridical and transformed working memory representations within unique coding schemes. *Imaging Neuroscience*, *2*, 1–20. https://doi.org/10.1162/imag_a_00173

Kandemir, G., Wilhelm, S. A., Axmacher, N., & Akyürek, E. G. (2024b). Maintenance of color memoranda in activity-quiescent working memory states: Evidence from impulse perturbation. *iScience*, *27*, 109565. https://doi.org/10.1016/j.isci.2024.109565

King, J. R., & Wyart, V. (2021). The human brain encodes a chronicle of visual events at each instant of time through the multiplexing of traveling waves. *Journal of Neuroscience*, *41*(34),7224-7233. https://doi.org/10.1523/JNEUROSCI.2098-20.2021

Kleiner, M., Brainard, D., Pelli, D., Ingling, A., Murray, R., & Broussard, C. (2007). What's new in Psychtoolbox-3. *Perception*, *36*(14), 1-16. https://doi.org/10.1068/v070821

Klimesch, W. (2012). α-band oscillations, attention, and controlled access to stored information. Trends in Cognitive Sciences, *16*(12), 606-17. https://doi.org/10.1016/j.tics.2012.10.007.

Kwak, Y., & Curtis, C. E. (2022). Unveiling the abstract format of mnemonic representations. Neuron, 110, 1822–1828. https://doi.org/10.1016/j.neuron.2022.03.016

Ledoit, O., & Wolf, M. (2004). Honey, I shrunk the sample covariance matrix. *The Journal of Portfolio Management*, *30*, 110–119. https://doi.org/10.3905/jpm.2004.110

Mostert, P., Albers, A. M., Brinkman, L., Todorova, L., Kok, P., & de Lange, F. P. (2018). Eye movement-related confounds in neural decoding of visual working memory representations. *eNeuro*, *5*(4), ENEURO.0401-17.2018. https://doi.org/10.1523/ENEURO.0401-17.2018

Myers, N. E., Stokes, M. G., & Nobre, A. C. (2017). Prioritizing information during working memory: Beyond sustained internal attention. *Trends in Cognitive Sciences*, *21*(6), 449–461. https://doi.org/10.1016/j.tics.2017.03.010

Myers, N. E., Rohenkohl, G., Wyart, V., Woolrich, M. W., Nobre, A. C., & Stokes, M. G. (2015). Testing sensory evidence against mnemonic templates. *eLife*, *4*, e09000. https://doi.org/10.7554/eLife.09000

Oberauer, K. (2002). Access to information in working memory: Exploring the focus of attention. *Journal of Experimental Psychology: Learning, Memory, and Cognition*, *28*(3), 411–421. https://doi.org/10.1037/0278-7393.28.3.411

Olivers, C. N. (2008). Interactions between visual working memory and visual attention. *Frontiers in Bioscience*, *13*(3), 1182-1191. https://doi.org/10.2741/2754

Olivers, C. N. L., Peters, J., Houtkamp, R., & Roelfsema, P. R. (2011). Different states in visual working memory: When it guides attention and when it does not. *Trends in Cognitive Sciences*, *15*(7),327-34. https://doi.org/10.1016/j.tics.2011.05.004.

Olivers, C. N. L., & Roelfsema, P. R. (2020). Attention for action in visual working memory. *Cortex*, *131*, 179–194. https://doi.org/10.1016/j.cortex.2020.07.011

Oostenveld, R., Fries, P., Maris, E., & Schoffelen, J.-M. (2011). FieldTrip: Open source software for advanced analysis of MEG, EEG, and invasive electrophysiological data.

Computational Intelligence and Neuroscience, *2011*, 156869. https://doi.org/10.1155/2011/156869.

Panichello, M. F., & Buschman, T. J. (2021). Shared mechanisms underlie the control of working memory and attention. *Nature*, *592*(7855), 601–605. https://doi.org/10.1038/s41586-021-03390-w

Pavlov, Y. G., & Kotchoubey, B. (2022). Oscillatory brain activity and maintenance of verbal and visual working memory: A systematic review. *Psychophysiology*, *59*, e13735. https://doi.org/10.1111/psyp.13735.

Pratte, M. S., & Tong, F. (2014). Spatial specificity of working memory representations in the early visual cortex. *Journal of Vision*, *14*(3), 22. https://doi.org/10.1167/14.3.22

Sassenhagen, J., & Draschkow, D. (2019). Cluster-based permutation tests of MEG/EEG data do not establish significance of effect latency or location. *Psychophysiology*, *56*(6), e13335. https://doi.org/10.1111/psyp.13335

Schneegans, S., & Bays, P. M. (2018). Drift in neural population activity causes working memory to deteriorate over time. *The Journal of Neuroscience*, *38*(21), 4859–4869. https://doi.org/10.1523/JNEUROSCI.3440-17.2018

Seki, K., Nakasato, N., Fujita, S., Hatanaka, K., Kawamura, T., Kanno, A., & Yoshimoto, T. (1996). Neuromagnetic evidence that the P100 component of the pattern reversal visual evoked response originates in the bottom of the calcarine fissure. *Electroencephalography and Clinical Neurophysiology*, *100*(5), 436–442. https://doi.org/10.1016/0168-5597(96)95098-4

Serences, J. T. (2016). Neural mechanisms of information storage in visual short-term memory. Vision Research, 128, 53–67. https://doi.org/10.1016/j.visres.2016.09.010

Serences, J. T., & Boynton, G. M. (2007). Feature-based attentional modulations in the absence of direct visual stimulation. *Neuron*, *55*(2), 301-12. https://doi.org/10.1016/j.neuron.2007.06.015

Serences, J. T., Ester, E. F., Vogel, E. K., & Awh, E. (2009). Stimulus-specific delay activity in human primary visual cortex. *Psychological Science*, *20*(2), 207–214. https://doi.org/10.1111/j.1467-9280.2009.02276.x

Stokes, M. G. (2015). "Activity-silent" working memory in prefrontal cortex: a dynamic coding framework. *Trends in Cognitive Sciences*, *19*(7), 394–405. https://doiorg/10.1016/j.tics.2015.05.004

van Driel, J., Günseli, E., Meeter, M., & Olivers, C. N. L. (2017). Local and interregional alpha EEG dynamics dissociate between memory for search and memory for recognition. *NeuroImage*, *149*, 114–128. https://doi.org/10.1016/j.neuroimage.2017.01.031

van Ede, F., Chekroud, S. R., Stokes, M. G., & Nobre, A. C. (2019). Concurrent visual and motor selection during visual working memory guided action. *Nature Neuroscience*, *22*(3), 477-483. https://doi.org/10.1038/s41593-018-0335-6.

van Ede, F., & Nobre, A. C. (2023). Turning Attention Inside Out: How Working Memory Serves Behavior. *Annual Review of Psychology*, *74*(1), 137–165. https://doi.org/10.1146/annurev-psych-021422-041757

Wolff, M. J., Jochim, J., Akyürek, E. G., & Stokes, M. G. (2017). Dynamic hidden states underlying working-memory-guided behavior. Nature Neuroscience, 20(6), 864–871. https://doi.org/10.1038/nn.4546

Wolff, M. J., Jochim, J., Akyürek, E. G., Buschman, T. J., & Stokes, M. G. (2020a). Drifting codes within a stable coding scheme for working memory. *PLoS Biology*, *18*(3), e3000625. https://doi.org/10.1371/journal.pbio.3000625.

Wolff, M. J., Kandemir, G., Stokes, M. G., & Akyürek, E. G. (2020b). Unimodal and bimodal access to sensory working memories by auditory and visual impulses. *The Journal of Neuroscience*, *40*(3), 671–681. https://doi.org/10.1523/JNEUROSCI.1194-19.2019

Supplements

The cross-location generalization during encoding was noisy for item 2 and did not reach statistical significance, despite the changes in signal were similar to Item 1, with emerging elevation in later stages. For item 1 this effect was statistically significant (Figure SA, Item 1, dark blue, 680 – 896 ms relative to item 1 onset, $p < 0.013$).

When post impulse period was investigated for Item 1 and 2 individually, both items reflected generalization across locations although the period at which this effect reached statistical significance differed (Figure SB, Item 1, dark blue, 192 – 304 ms relative to impulse 1 onset, $p < 0.034$; Item 2, orange, 408 – 560 ms relative to impulse 1 onset, $p < 0.027$).

Figure S1

Time-course generalization of Item 1 and Item 2 representations across locations during encoding (A), and maintenance (B).

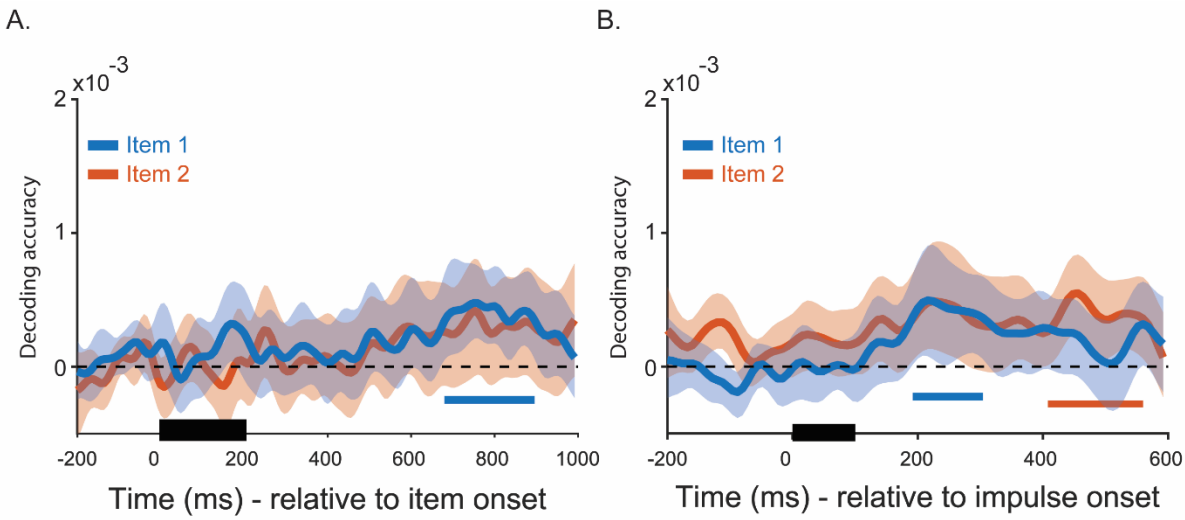

Note. The generalization of neural code for memory item 1 (dark blue) and Item 2 (orange) across locations relative to the onset of item 1 and 2 (A) and relative to impulse 1 and 2 (B). **A-B.** The solid line represents the mean decoding accuracy when training on one spatial location (e.g. left) and testing on other (e.g. right) as a function of time. Shades around solid lines mark 95 % C.I. Solid bars below baseline reflect the time-window with statistically significant decoding according to cluster-based permutation test ($p < 0.05$).

Figure S2

Generalization of neural code across memory item 1 and 2 at the same and distinct locations as a function of time.

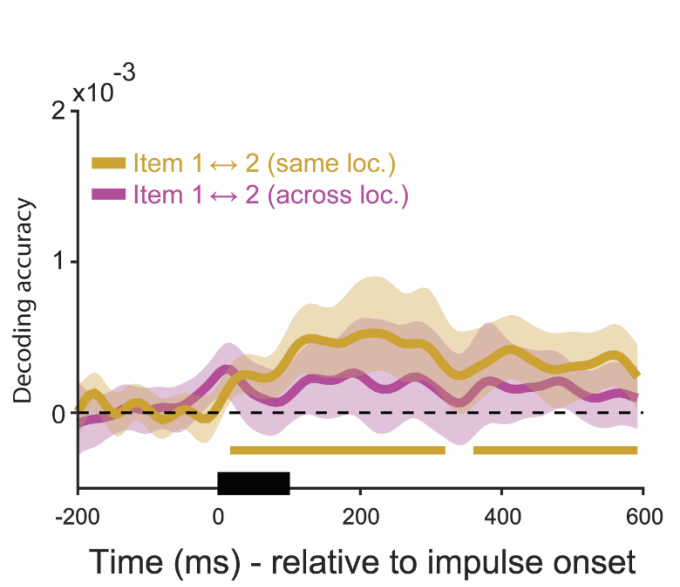

Note. The generalization of neural code across memory items during the maintenance following the presentation of impulse 1 and 2. Solid lines mark mean decoding accuracy when training on Item 1 and testing on Item 2 (mustard), and testing on Item 2 at cross-location (pink)A-B. Shades around solid lines mark 95 % C.I. Solid bars below baseline reflect the time-window with statistically significant decoding according to cluster-based permutation test ($p < 0.05$).

We also assessed the generalization of neural code across items following impulse 1 and 2 presentation. The representations of recently encoded memories reacted similarly to impulse perturbation, reflecting comparable neural signature (Figure S2, Item 1 ↔ 2 same loc., yellow, 16 - 312 ms and 360- 592 ms relative to Impulse 1 & 2 onset, $p = 0.006$ & $p = 0.013$). On the other hand, this similarity was not strong enough to generalize across locations when the neural code for Item 1 was tested on item 2 at another location (Figure S2, Item 1 ↔ 2 across loc., pink, $p > 0.05$). It is likely that this generalization mainly fails due to weaker neural signal evoked by impulse perturbation.